Clin Neuroradiol (2019) 29:277–284
https://doi.org/10.1007/s00062-017-0644-2

ORIGINAL ARTICLE

Reduction of Metallic Artifacts of the Post-treatment Intracranial Aneurysms: Effects of Single Energy Metal Artifact Reduction Algorithm

Yu-Ning Pan[1] · Ge Chen[2] · Ai-Jing Li[3] · Zhao-Qian Chen[1] · Xiang Gao[4] · Yi Huang[4] · Bradley Mattson[5] · Shan Li[5]

Received: 5 September 2017 / Accepted: 24 October 2017 / Published online: 16 November 2017

Abstract
Purpose This study evaluated the quality of computed tomography (CT) and CT angiography images generated using the single-energy metal artifact reduction (SEMAR) algorithm during perfusion examination in patients who had undergone reconstruction with neurosurgical clipping or endovascular coiling for treatment of aneurysms.
Methods A total of 55 patients with implanted intracranial clips or coils (24 men and 31 women; mean age 60.15 ± 15.86 years) underwent perfusion studies evaluated by CT and CT angiography with a 320-row CT scanner. Images were reconstructed with either the SEMAR algorithm combined with iterative reconstruction (SEMAR group), or by iterative reconstruction only (non-SEMAR group control). The SEMAR and control images were compared for artifacts (index and maximum diameter), image quality, cerebral perfusion parameters, noise (images with the worst artifacts), and contrast-to-noise ratio. The metallic artifacts were visually evaluated by two radiologists using a four-point scale in a double-blinded manner.
Results The noise, artifact diameter, and artifact index of the SEMAR images were significantly lower than that of the control images, and the subjective image quality score and contrast-to-noise ratio were significantly higher ($P < 0.01$, all). The cerebral perfusion parameters of the SEMAR and control images were comparable (i. e. blood flow, blood volume, and mean transit time).
Conclusion For imaging intracranial metallic implants, the SEMAR algorithm produced images with significantly fewer artifacts than the iterative reconstruction alone, with no statistical changes in perfusion parameters. Thus, SEMAR reconstruction can be instrumental in improving CT image quality and may ultimately improve the detection of postoperative complications and patient prognosis.

Keywords Metallic artifact · Image quality · Computed tomography angiography · Noise · Perfusion

Electronic supplementary material The online version of this article (https://doi.org/10.1007/s00062-017-0644-2) contains supplementary material, which is available to authorized users.

✉ Ai-Jing Li
lajnbey@163.com

[1] Department of Radiology, Ningbo First Hospital, Ningbo Hospital, Zhejiang University, 315010 Ningbo, Zhejiang, China

[2] Department of Clinical medical engineering Ningbo First Hospital, Ningbo Hospital, Zhejiang University, 315010 Ningbo, Zhejiang, China

[3] Department of Radiology, Ningbo No. 2 Hospital, 315010 Ningbo, Zhejiang, China

[4] Department of Neurosurgery, Ningbo First Hospital, Ningbo Hospital, Zhejiang University, 315010 Ningbo, Zhejiang, China

[5] Department of Radiology, Baystate Medical Center, University of Massachusetts School of Medicine, Springfield, MA 01199, USA

Introduction

Intracranial aneurysms are a relatively common cerebrovascular disorder affecting approximately 4% of the general population [1, 2]. Neurosurgical clipping and endovascular coiling are the primary treatment options for ruptured intracranial aneurysms. Patients then undergo regular routine monitoring to assess the curative effect of treatment, and screen for possible postoperative complications [3, 4]. Neuroimaging techniques including digital subtraction angiography (DSA), magnetic resonance imaging (MRI), and

computed tomography angiography (CTA) are essential for evaluating and treating patients with intracranial aneurysms. The DSA is a well-established imaging technique used for monitoring the efficacy of aneurysm clipping or coiling [1]; however, it is invasive and can only be used to evaluate the brain vasculature [4]. Metallic implants disrupt the homogeneity of magnetic fields; therefore, the efficacy of MRI is limited by the large artifact area surrounding the metallic implant, as well as the risk of its displacement by the magnetic field [5]. Similarly, the diagnostic value of conventional computed tomography (CT) is hampered by metallic artifacts [6]. With improvements in spatial and temporal resolutions, multi-detector CT cerebral angiography has been accepted for evaluating outcomes and complications of clipping or endovascular coiling of cerebral aneurysms [3]. Nevertheless, metallic implants affect image quality [7]. A beam-hardening artifact obscures the surrounding anatomical structures, affecting the evaluation of postoperative complications and aneurysm recurrence [4]. Therefore, it is crucial to minimize the influence of metallic artifacts on imaging results.

In recent years several technologies have been introduced that reduce metallic artifacts, without satisfactory results [6, 8]. These include energy spectrum CT and postprocessing methods. In addition, cerebral perfusion parameters have been used to evaluate treatment of intracranial aneurysm, but few studies have examined the influence of small intracranial metallic implants on cerebral perfusion parameters [9, 10].

Dual-energy CT can be used to reduce the area of metallic artifact after a single high-KeV energy reconstruction; however, the surrounding structures may become blurred, affecting the cerebral perfusion parameters [9]. To reduce the influence of metal implants on CT images, an algorithm for single-energy metal artifact reduction (SEMAR) was recently introduced on a second-generation 320-row CT scanner [11, 12]. Previous studies have examined the ability of the SEMAR algorithm to reduce large metallic artifacts on CT images in patients with hip, spinal, and dental implants [13–15]; however, the extent of metallic artifacts differs significantly according to the size and shape of the implants [16]. Additionally, there are no available studies that examined the effect of the SEMAR algorithm on cerebral perfusion parameters. In the current study, we evaluated the efficiency of the SEMAR reconstruction algorithm for reducing image artifacts resulting from intracranial implants and the effect of this algorithm on cerebral perfusion parameters. To the best of our knowledge, this is the first study to address these issues.

Methods

Patients

A total of 55 patients (24 men and 31 women; mean age 60.15 ± 15.86 years) with metallic brain implants underwent 320-row CTA imaging from August 2016 to December 2016 in the Ningbo First Hospital. Of the patients two had CTA performed twice; therefore in this study, we retrospectively examined the results of 57 CTA images.

Of the 55 patients 17 underwent neurosurgical clipping. Specifically, there were 3, 9, 3, and 2 aneurysm cases that involved the anterior cerebral, middle cerebral, anterior communicating, and posterior communicating arteries, respectively. The remaining 38 patients underwent coil embolization: 7, 12, and 13 patients had aneurysms involving the anterior cerebral, middle cerebral, and anterior communicating arteries, respectively, and 2 patients each had aneurysms in the posterior communicating, internal carotid, and vertebral arteries. Patients with any of the following were excluded: allergy to iodine contrast agent, pregnancy, severe cardiovascular disease, or severe renal insufficiency (creatinine clearance $\leq$120 μmol/l).

Scanning Parameters

Contrast-enhanced CTA images were obtained on a second-generation 320-row CT scanner (Aquilion ONE, Toshiba Medical Systems, Otawara, Japan). The patients' heads were straightened and secured in place with a belt. The anon-spiral scanning mode was used for CTA examination. The imaging acquisition parameters were: tube rotation time 0.5 s at 80 kVp and 150 mA, scanning range 16 cm, slice thickness 0.5 mm and field of view 24 cm.

A bolus injection of Ultravist (370 mg/ml; Bayer-Schering Healthcare, Berlin, Germany) was administered intravenously with a high-pressure injector (Stellant-Dual Flow, Medrad, Pittsburgh, PA, USA) at a dose of 1.0 ml/kg and rate of 5.0 ml/s, followed by a 20 ml saline flush at the same rate. Subsequently, a 19 rotation dynamic volume scanning protocol was performed (Suppl. Fig. 1).

Image Reconstruction

Raw data images were reconstructed using two different reconstruction methods, which constituted the treatment groups compared in this study, that is, the SEMAR and the non-SEMAR control groups. In both the SEMAR and control groups, the adaptive iterative reconstruction (AIDR) algorithm (AIDR 3D50%; Toshiba) was applied. In the SEMAR group only, the AIDR 3D algorithm was combined with the SEMAR algorithm (Toshiba) to reconstruct the SEMAR images. All raw images were postprocessed on an

independent postprocessing workstation (Vitrea fx version 1.0, Vital Images, Minnetonka, MN, USA). The selected reference arterial input function was the middle cerebral artery and the reference venous output function was the superior sagittal sinus. The dynamic time density curve and color perfusion parametric maps were automatically obtained from the software. The perfusion parameters included regional cerebral blood flow, regional cerebral blood volume, and mean transit time.

Evaluation of Image Quality

Subjective Evaluation of Image Quality

All images were graded by two experienced radiologists with at least 7–9 years of experience in the field of neuroradiology. The radiologists were blinded to the patients' identity. The image quality was graded according to the degree of perceived metallic artifacts, as described previously [17]. Briefly, image quality was graded as follows: 1) extensive artifacts, images could not provide diagnostic information, 2) strong artifacts, images provided limited diagnostic information, 3) mild artifacts, good images that provided sufficient diagnostic information and 4) minimal artifacts, excellent images that provided very useful diagnostic information.

Objective Evaluation of Image Quality

To avoid the influence of the contrast medium, data of the images with the worst artifacts were selected from each patient to evaluate image quality. The window width was set to 100 Hounsfield units (HU), the window level was set to 40HU and 5 regions of interest (ROIs) with a radius of ~1 cm and interval of 72° were selected, focusing on the metal artifacts. The CT value and standard deviations (SD) of these five ROIs were measured.

The CT value and SD of surrounding structures at the same level without artifacts were measured and used as the reference. In the same patient, the measurement location and scope were consistent with an area of approximately80 mm^2 and the ROI avoided the skull and air as much as possible (Fig. 1). The average SD of the ROI was set as the image noise. The diameter of artifacts was defined as the length of the dark zone caused by beam hardening [18] and the largest diameter was measured in the cross-sectional image.

The artifact index (AI) and contrast-to-noise ratio (CNR) were calculated using the following formulas:

$$AI = \sqrt{SD^2_{artifact} - SD^2_{reference}};$$

$$CNR = \frac{|CT_{artificate} - CT_{reference}|}{\sqrt{\left(SD^2_{artifact} - SD^2_{reference}\right)/2}}$$

Evaluation of the Perfusion Parameters

Identical slice locations were selected at the level of the basal ganglia in all the perfusion studies performed with both the SEMAR and non-SEMAR algorithms. The five identical ROIs were placed in the bilateral frontal lobes gray and white matter, putamen and the temporal lobes gray and white matter. Each ROI measured approximately 10 mm^2 and each was located outside the blood vessels, lesion, and metallic artifact areas. The perfusion parameters (cerebral blood flow, cerebral blood volume and mean transit time) were calculated for each ROI.

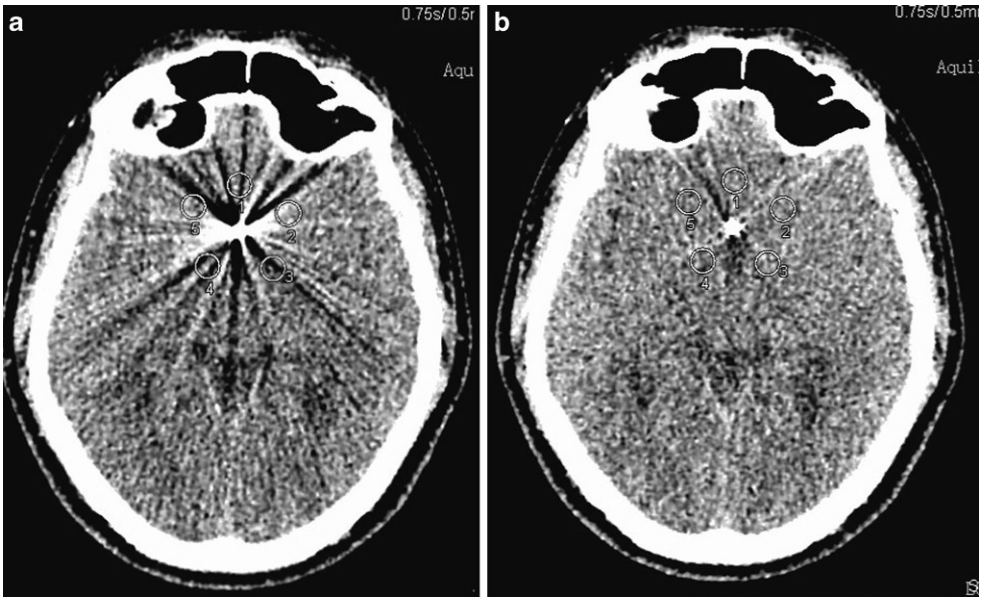

Fig. 1 Objective image parameters were measured on an original non-SEMAR (single-energy metal artifact reduction) image (**a**) and SEMAR image (**b**) in 0.5 mm slice thickness and five regions of interest (ROIs) were designated around the metallic implants. The ROI setting was consistent between the non-SEMAR and SEMAR groups. The CT values and the standard deviations of surrounding structures without artifact were measured as a reference

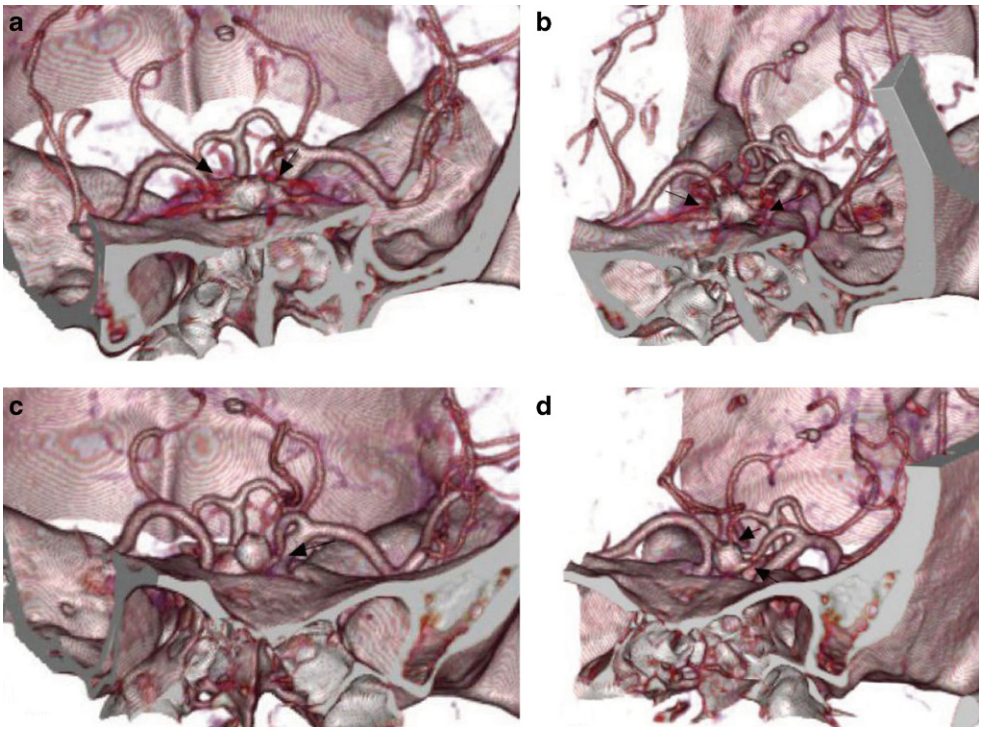

Fig. 2 A 68-year-old male with an anterior communicating aneurysm 3 months post-coil embolization. **a**,**b** Non-SEMAR (single-energy metal artifact reduction) images: the coils produce severe metallic artifact (*arrows*) and the surrounding structures are not well visualized (subjective image quality score = 1). **c**,**d** SEMAR images: there are no perceptible artifacts around coils and the adjacent vascular structures are clearly demonstrated without evidence of aneurysm recurrence or stenosis in the blood vessels feeding the aneurysm (*black arrows*; subjective image quality score = 4)

Statistical Analysis

The objective evaluation of image quality between non-SEMAR and SEMAR groups were compared using the Mann-Whitney U-test. The kappa test was used to compare the consistency of the assessments of the two radiologists involved in the study. Kappa values of 0.81–1.00, 0.61–0.80, 0.41–0.60, and <0.40 indicated a very strong, strong, moderate, and poor fit, respectively.

The image noiseAI, CNR, and the maximum diameter of artifacts were compared using a paired Student's *t*-test between the SEMAR and control groups. Pearson's correlation coefficient was used to analyze the correlation between the perfusion parameters of each of the two algorithms. Statistical analyses were performed using SPSS version 19.0. All the data are shown as mean± standard deviation. $P < 0.05$ was considered statistically significant.

Table 1 Objective evaluation scores of the SEMAR and the non-SEMAR groups ($n = 57$, each)

	Non-SEMAR	SEMAR
Image noise, HU	60.04 ± 21.68	24.86 ± 11.29
Maximum diameter of artifacts, mm	132.58 ± 33.29	7.47 ± 7.04
Artifact index, HU	56.18 ± 16.61	21.05 ± 8.54
Contrast-to-noise ratio	3.09 ± 1.26	12.46 ± 3.14

$P = 0.001$, each comparison, *HU* Hounsfield Unit, *SEMAR* single-energy metal artifact reduction

Results

Subjective Evaluation of Image Quality

The SEMAR images contained significantly fewer metallic artifacts compared with the non-SEMAR images, and image quality was also significantly better ($P < 0.001$, each). The subjective score for image quality of the SEMAR group (3.77 ± 0.42) was significantly higher than that of the non-SEMAR group (1.08 ± 0.29, $P < 0.001$). The consistency of the scores between the two radiologists was high (kappa=0.82, $P < 0.05$).

Objective Evaluation of Image Quality

Each of the objective evaluation scores (for noise, maximum diameter of artifacts, AI, and CNR) of the SEMAR and non-SEMAR images differed significantly ($P < 0.001$; Table 1). Specifically, the image noise, maximum diameter of artifacts, and AI of the SEMAR images were each significantly less than that of the non-SEMAR group, while the CNR was significantly higher. Representative images from a 68-year-old man and a 77-year-old woman reconstructed by SEMAR and non-SEMAR algorithms are shown in Figs. 2 and 3, respectively. The SEMAR image reconstructions yielded obviously fewer artifacts and better image quality relative to the non-SEMAR images (Fig. 2c and d; Fig. 3c, d and f).

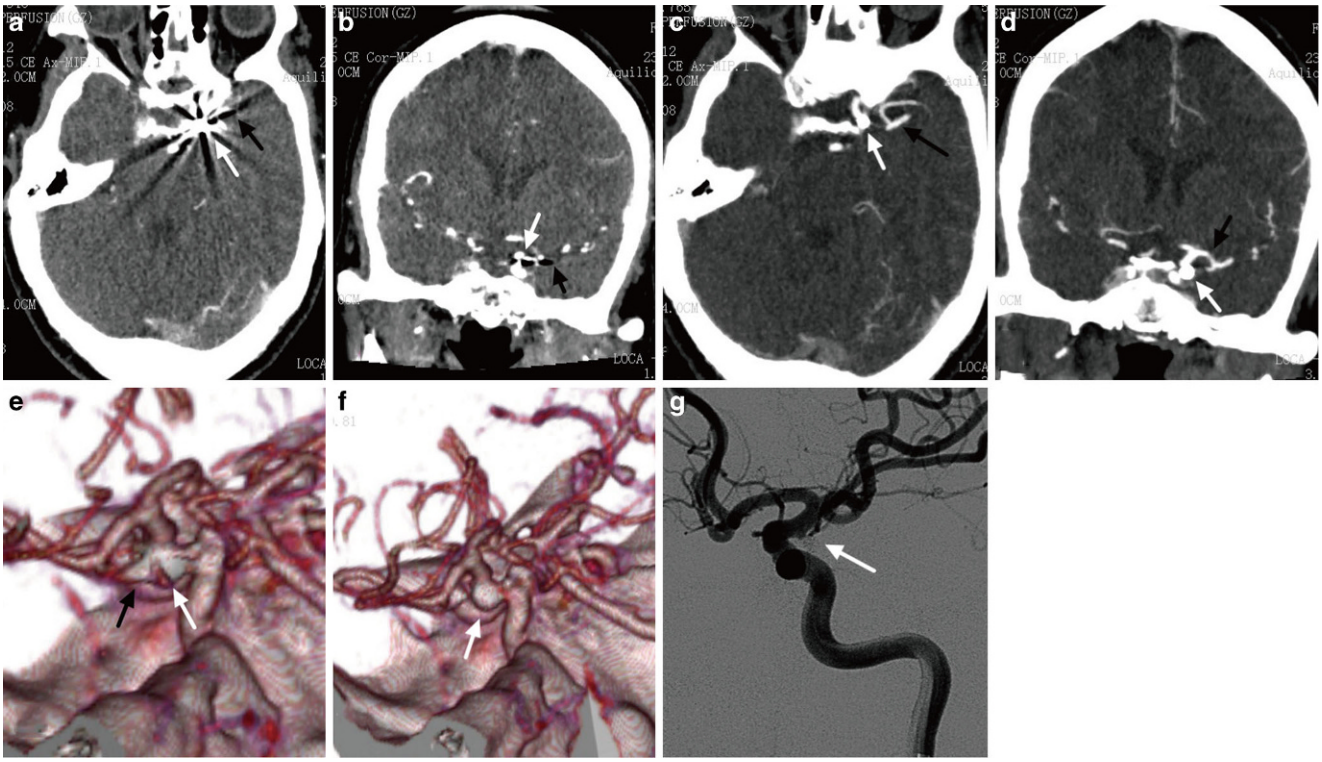

Fig. 3 A 77-year-old female with a posterior communicating aneurysm 6 months post-coil embolization. Non-SEMAR (single-energy metal artifact reduction) axial (**a**) and coronal images (**b**) demonstrating the presence of strong metallic artifacts around the coiled aneurysm (*white arrow*), the surrounding structure is obscure, like the middle cerebral artery (*black arrow*). SEMAR axial (**c**) and coronal images (**d**) showing complete occlusion of the aneurysm with substantially reduced metallic artifacts (*white arrow*), the surrounding structure is clear, as the middle cerebral artery (*black arrow*). The non-SEMAR images (**e**) showing several artifacts like sharp corns which can be misdiagnosed as residual or aneurysm recurrence. The SEMAR images (**f**) demonstrating no artifacts, the aneurysm has been embolized and the same findings were verified by digital subtraction angiography (**g**)

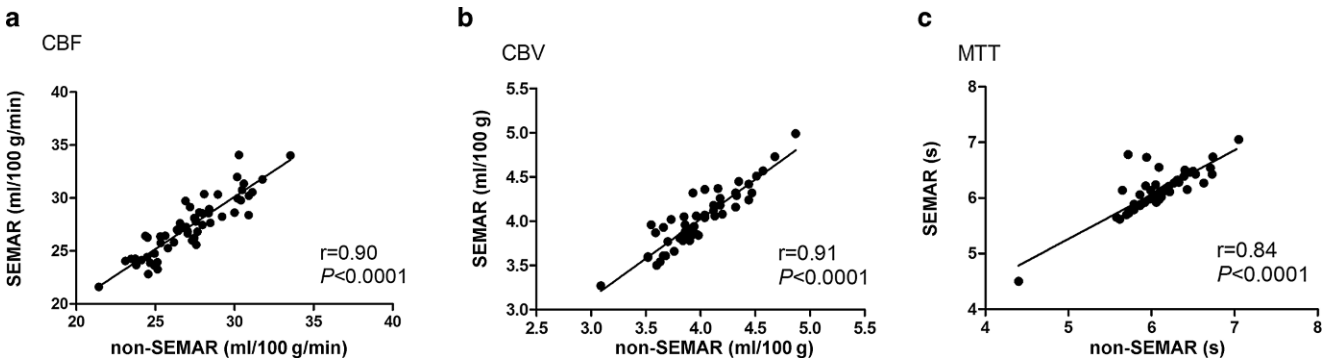

Fig. 4 Scatter diagrams of the mean values obtained from all regions of interest. Linear correlation was observed between the non-SEMAR (single-energy metal artifact reduction) and SEMAR groups with respect to mean cerebral blood flow (CBF, units for X- and Y-axes: ml/100 g/min) (**a**), mean cerebral blood volume (CBV, units for X- and Y-axes: ml/100 g) (**b**), mean transit time (MTT, units for X- and Y-axes: s) (**c**)

Perfusion Evaluation

Pearson's correlation coefficient showed a significant positive correlation between the non-SEMAR and non-SEMAR images and cerebral blood flow, cerebral blood volume, and mean transit time ($P < 0.0001$, Tables 2, 3 and 4, respectively). The mean perfusion values in the SEMAR and non-SEMAR groups exhibited a linear correlation (Fig. 4a–c). The color parametric maps obtained from both algorithms did not show significant differences.

Table 2 Correlation between non-SEMAR and SEMAR groups with respect to mean cerebral blood flow (ml/100 g/min)

		Non-SEMAR	SEMAR	*r*
Right	Frontal gray matter	30.91 ± 4.74	30.57 ± 4.54	0.79
	Frontal white matter	23.72 ± 5.48	23.29 ± 5.89	0.93
	Putamen	31.10 ± 4.78	30.26 ± 4.98	0.86
	Temporal gray matter	27.46 ± 6.25	28.73 ± 5.87	0.71
	Temporal white matter	21.23 ± 5.48	24.50 ± 6.81	0.85
Left	Frontal gray matter	31.21 ± 5.16	30.67 ± 5.08	0.88
	Frontal white matter	22.77 ± 5.05	23.05 ± 4.77	0.89
	Putamen	31.73 ± 4.80	32.14 ± 4.73	0.80
	Temporal gray matter	27.93 ± 6.19	27.46 ± 6.25	0.75
	Temporal white matter	23.81 ± 6.89	24.69 ± 6.59	0.74

$P < 0.0001$ non-SEMAR cf. SEMAR, in each region of interest, *SEMAR* single-energy metal artifact reduction

Table 3 Cerebral blood volume of the non-SEMAR and SEMAR groups (ml/100 g)

		Non-SEMAR	SEMAR	*r*
Right	Frontal gray matter	3.91 ± 0.69	3.92 ± 0.67	0.87
	Frontal white matter	3.52 ± 0.56	3.50 ± 0.61	0.92
	Putamen	5.12 ± 0.69	5.16 ± 0.67	0.93
	Temporal gray matter	3.74 ± 0.68	3.81 ± 0.56	0.78
	Temporal white matter	3.56 ± 0.54	3.59 ± 0.56	0.87
Left	Frontal gray matter	3.84 ± 0.72	3.86 ± 0.66	0.76
	Frontal white matter	3.57 ± 0.47	3.61 ± 0.51	0.79
	Putamen	5.21 ± 0.83	5.24 ± 0.81	0.65
	Temporal gray matter	3.72 ± 0.58	3.77 ± 0.57	0.80
	Temporal white matter	3.62 ± 0.57	3.64 ± 0.59	0.90

$P < 0.0001$ non-SEMAR cf. SEMAR, in each region of interest, *SEMAR* single-energy metal artifact reduction

Table 4 Mean transit time of the non-SEMAR and SEMAR groups (seconds)

		Non-SEMAR	SEMAR	*r*
Right	Frontal gray matter	6.19 ± 1.23	6.35 ± 1.16	0.78
	Frontal white matter	6.18 ± 1.24	6.22 ± 1.15	0.72
	Putamen	5.99 ± 1.08	6.00 ± 1.06	0.92
	Temporal gray matter	6.14 ± 1.27	6.29 ± 1.36	0.80
	Temporal white matter	6.17 ± 1.23	6.25 ± 1.12	0.82
Left	Frontal gray matter	5.96 ± 1.08	6.12 ± 1.13	0.67
	Frontal white matter	6.17 ± 1.16	6.19 ± 1.14	0.89
	Putamen	6.00 ± 1.11	6.07 ± 1.09	0.72
	Temporal gray matter	6.11 ± 1.36	6.17 ± 1.32	0.95
	Temporal white matter	6.10 ± 1.12	6.08 ± 1.17	0.89

$P < 0.0001$ non-SEMAR cf. SEMAR, in each region of interest, *SEMAR* single-energy metal artifact reduction

Discussion

Metallic artifacts often obscure CT images and pose a challenge for accurate postoperative evaluation and follow-up [6, 19]. The AIDR 3D algorithm reduces image noise, but metallic artifacts remain [11, 20]. Therefore, in this study, we determined whether the SEMAR algorithm, used in conjunction with the AIDR 3D, could improve CT images by reducing metal artifacts as well as image noise. Specifically, we compared the metallic artifacts and perfusion parameters of images obtained using both the AIDR 3D and SEMAR reconstruction algorithms (the SEMAR group) with that obtained with only the AIDR 3D algorithm (non-SEMAR control group). We determined that both the objective and subjective quality of images of the cerebral arteries after aneurysm clipping or coiling was improved by addition of the SEMAR algorithm reconstruction. Compared with the control group, images that underwent SEMAR reconstruc-

tion had significantly less noise, lower AI and maximum diameter of artifacts, and significantly higher CNR and subjective scores for image quality. The decrease in intracranial metallic artifacts improved visualization of the surrounding structures and detection of postoperative complications.

Accurate evaluation of the cerebral perfusion parameters can directly influence accurate prediction of patient prognosis [10, 21]. In the present study, the SEMAR reconstruction significantly improved the image quality without affecting the perfusion parameters, as there were no significant differences in perfusion parameters between the SEMAR and control images.

To date, the techniques used to suppress metallic artifacts during image postprocessing can be broadly classified as projection interpolation, iterative reconstruction, or a hybrid combination of both techniques. The projection interpolation method is generally based on the filtered back projection algorithm. It can significantly reduce artifacts resulting from large metallic implants, but the image noise is higher in the area surrounding the implant [9, 10]. On the other hand, the iterative reconstruction algorithm can reduce large metallic artifacts and suppress image noise, but its high computational complexity makes the process slow and impractical for wide clinical use [22]. The hybrid method is based on the framework of the interpolation method, but utilizes iterative reconstruction on reconstructing metallic artifacts [23, 24]. Compared with iterative reconstruction the hybrid method has faster processing times and better visualization of metallic objects; however, the structures surrounding the metallic implants are often distorted; therefore, its practical application is significantly limited [24].

The SEMAR algorithm used in the present study is based on the filtered back projection algorithm [11, 12]. We did not observe an increase in image noise after the SEMAR reconstruction, which can be attributed to the efficiency of the SEMAR algorithm for removing metal artifacts or the distal distance between the intracranial implant and the surrounding air. In addition, the reconstruction time needed for the application of the SEMAR algorithm is relatively fast [14]. In the non-SEMAR control group, the processing time for image construction was close to real-time imaging in our workstation, whereas, in the SEMAR group, the reconstruction time was 5–10 min. Furthermore, the SEMAR algorithm did not affect areas that had no metallic artifacts. Therefore, we did not observe significant differences in perfusion parameters between the SEMAR and non-SEMAR groups. In good agreement, Korpics et al. previously reported that in images of the head and neck, CT attenuation and image noise were similar in regions without metallic artifacts, before and after SEMAR reconstruction [20].

Energy spectrum CT uses a single constant tube voltage that produces electrons with a single photon energy, resulting in high-resolution images and low radiation exposure. Energy spectrum CT aims to minimize artifacts and improve image quality during data acquisition, rather than using a postprocessing software algorithm; however, due to manufacturing limitations, energy spectrum CT cannot completely remove metallic artifacts caused by beam hardening, and corrections for large metallic artifacts tend to overcompensate [9, 25]. In addition, several other factors contribute to producing metallic artifacts, including the electronic hunger effect, partial volume, noise, scattering, and artifacts due to motion. Another consideration is that energy spectrum CT requires a dual-source CT scanner with a detailed scan scheme, and currently there is no consensus regarding the optimal kVp used with dual-source CT [26]. On the other hand, SEMAR is a postprocessing algorithm based on raw data and a single-energy pattern [14, 27]. In SEMAR reconstructed images, data collection is similar to that of routine scanning and metallic artifacts can be removed later in postprocessing. Therefore, the SEMAR algorithm can be applied retrospectively on routine CT scanning. Furthermore, the SEMAR algorithm can be used for axial scanning, and it is being studied for spiral scanning. Therefore, only areas within a scanning length of 16 cm can be evaluated [11, 12, 14].

This study had a few limitations. First, we found that the SEMAR algorithm could successfully improve the image quality in almost all examined patients without compromising the image quality or hiding important findings. Moreover, most patients had a definite diagnosis with CTA, and we did not have to compare its use to the DSA technique; however, we will make sure to address the diagnostic performance of the SEMAR algorithm in future studies. Second, our study was performed using one tube voltage (80 kV) and we did not examine the association between radiation dose and artifacts. Third, we did not study the influence of the implant material on the resulting artifacts and image quality. Finally, we did not compare the SEMAR algorithm with other metallic artifact reduction algorithms. Therefore, future studies are necessary to validate the results obtained here.

Conclusion

The results of this study demonstrated the effectiveness of the SEMAR reconstruction algorithm for reducing metallic artifacts generated from intracranial aneurysm clips and endovascular coils, without affecting the perfusion parameters. Consequently, this allowed better visualization of the surrounding structures and improved detection of postoperative complications.

Acknowledgements This work was supported by the Project of Medical and Health Technology Program of Zhejiang Province (2018KY155), the Huimin Project of Science and Technology of Ningbo City (2016C51013), the Natural Science Foundation Project of Ningbo City (2016A610140), Ningbo People of Science and Technology Projects (2015C50005) and the National Key Research and Development Plan (2016YFC0106106).

Compliance with ethical guidelines

Conflict of interest Y.-N. Pan, G. Chen, A.-J. Li, Z.-Q. Chen, X. Gao, Y. Huang, B. Mattson and S. Li declare that they have no competing interests.

Ethical standards The Ethics Committee of Ningbo First Hospital approved this retrospective study.

References

1. Keedy A. An overview of intracranial aneurysms. Mcgill J Med. 2006;9:141–6.
2. Morita A, Kimura T, Shojima M, Sameshima T, Nishihara T. Unruptured intracranial aneurysms: current perspectives on the origin and natural course, and quest for standards in the management strategy. Neurol Med Chir (Tokyo). 2010;50:777–87.
3. Shapiro M, Ollenschleger MD, Baccin C, Becske T, Spiegel GR, Wang Y, Song X, Raz E, Zumofen D, Potts MB, Nelson PK. Foreign body emboli following cerebrovascular interventions: clinical, radiographic, and histopathologic features. AJNR Am J Neuroradiol. 2015;36:2121–6.
4. Bharatha A, Yeung R, Durant D, Fox AJ, Aviv RI, Howard P, Thompson AL, Bartlett ES, Symons SP. Comparison of computed tomography angiography with digital subtraction angiography in the assessment of clipped intracranial aneurysms. J Comput Assist Tomogr. 2010;34:440–5.
5. Friedrich B, Wostrack M, Ringel F, Ryang YM, Forschler A, Waldt S, Zimmer C, Nittka M, Preibisch C. Novel metal artifact reduction techniques with use of slice-encoding metal artifact correction and view-angle tilting MR imaging for improved visualization of brain tissue near intracranial aneurysm clips. Clin Neuroradiol. 2016;26:31–7.
6. Barrett JF, Keat N. Artifacts in CT: recognition and avoidance. Radiographics. 2004;24:1679–91.
7. Lee MJ, Kim S, Lee SA, Song HT, Huh YM, Kim DH, Han SH, Suh JS. Overcoming artifacts from metallic orthopedic implants at high-field-strength MR imaging and multi-detector CT. Radiographics. 2007;27:791–803.
8. Fang J, Zhang D, Wilcox C, Heidinger B, Raptopoulos V, Brook A, Brook OR. Metal implants on CT: comparison of iterative reconstruction algorithms for reduction of metal artifacts with single energy and spectral CT scanning in a phantom model. Abdom Radiol (NY). 2017;42(3):742–8.
9. Morsbach F, Wurnig M, Kunz DM, Krauss A, Schmidt B, Kollias SS, Alkadhi H. Metal artefact reduction from dental hardware in carotid CT angiography using iterative reconstructions. Eur Radiol. 2013;23:2687–94.
10. Morsbach F, Bickelhaupt S, Wanner GA, Krauss A, Schmidt B, Alkadhi H. Reduction of metal artifacts from hip prostheses on CT images of the pelvis: value of iterative reconstructions. Radiology. 2013;268:237–44.
11. Funama Y, Taguchi K, Utsunomiya D, Oda S, Hirata K, Yuki H, Kidoh M, Hatemura M, Yamashita Y. A newly-developed metal artifact reduction algorithm improves the visibility of oral cavity lesions on 320-MDCT volume scans. Phys Med. 2015;31:66–71.
12. Kidoh M, Utsunomiya D, Ikeda O, Tamura Y, Oda S, Funama Y, Yuki H, Nakaura T, Kawano T, Hirai T, Yamashita Y. Reduction of metallic coil artefacts in computed tomography body imaging: effects of a new single-energy metal artefact reduction algorithm. Eur Radiol. 2016;26:1378–86.
13. Sonoda A, Nitta N, Ushio N, Nagatani Y, Okumura N, Otani H, Murata K. Evaluation of the quality of CT images acquired with the single energy metal artifact reduction (SEMAR) algorithm in patients with hip and dental prostheses and aneurysm embolization coils. Jpn J Radiol. 2015;33:710–6.
14. Yasaka K, Maeda E, Hanaoka S, Katsura M, Sato J, Ohtomo K. Single-energy metal artifact reduction for helical computed tomography of the pelvis in patients with metal hip prostheses. Jpn J Radiol. 2016;34:625–32.
15. Gondim Teixeira PA, Meyer JB, Baumann C, Raymond A, Sirveaux F, Coudane H, Blum A. Total hip prosthesis CT with single-energy projection-based metallic artifact reduction: impact on the visualization of specific periprosthetic soft tissue structures. Skeletal Radiol. 2014;43:1237–46.
16. Douglas-Akinwande AC, Buckwalter KA, Rydberg J, Rankin JL, Choplin RH. Multichannel CT: evaluating the spine in postoperative patients with orthopedic hardware. Radiographics. 2006;26(Suppl 1):S97–S110.
17. Brook OR, Gourtsoyianni S, Brook A, Mahadevan A, Wilcox C, Raptopoulos V. Spectral CT with metal artifacts reduction software for improvement of tumor visibility in the vicinity of gold fiducial markers. Radiology. 2012;263:696–705.
18. Geisel D, Gebauer B, Malinowski M, Stockmann M, Denecke T. Comparison of CT and MRI artefacts from coils and vascular plugs used for portal vein embolization. Eur J Radiol. 2014;83:692–5.
19. Venema HW, den Heeten GJ. Subtraction helical CT angiography of intra- and extracranial vessels: technical considerations and preliminary experience – rediscovery of matched mask bone elimination? AJNR Am J Neuroradiol. 2003;24(2):1491.
20. Korpics M, Surucu M, Mescioglu I, Alite F, Block AM, Choi M, Emami B, Harkenrider MM, Solanki AA, Roeske JC. Observer evaluation of a metal artifact reduction algorithm applied to head and neck cone beam computed tomographic images. Int J Radiat Oncol Biol Phys. 2016;96:897–904.
21. Orrison WW Jr., Snyder KV, Hopkins LN, Roach CJ, Ringdahl EN, Nazir R, Hanson EH. Whole-brain dynamic CT angiography and perfusion imaging. Clin Radiol. 2011;66:566–74.
22. Hudson HM, Larkin RS. Accelerated image reconstruction using ordered subsets of projection data. IEEE Trans Med Imaging. 1994;13:601–9.
23. Lemmens C, Faul D, Nuyts J. Suppression of metal artifacts in CT using a reconstruction procedure that combines MAP and projection completion. IEEE Trans Med Imaging. 2009;28:250–60.
24. Van Slambrouck K, Nuyts J. Metal artifact reduction in computed tomography using local models in an image block-iterative scheme. Med Phys. 2012;39:7080–93.
25. Kuchenbecker S, Faby S, Sawall S, Lell M, Kachelriess M. Dual energy CT: how well can pseudo-monochromatic imaging reduce metal artifacts? Med Phys. 2015;42:1023–36.
26. Yu L, Christner JA, Leng S, Wang J, Fletcher JG, McCollough CH. Virtual monochromatic imaging in dual-source dual-energy CT: radiation dose and image quality. Med Phys. 2011;38:6371–9.
27. Weiss J, Schabel C, Bongers M, Raupach R, Clasen S, Notohamiprodjo M, Nikolaou K, Bamberg F. Impact of iterative metal artifact reduction on diagnostic image quality in patients with dental hardware. Acta Radiol. 2016;58(3):279–85.